



## **On the Strength and DSM Design of Cold-Formed Steel Web/Flange-Stiffened Lipped Channel Columns Buckling in Distortional Modes**

Alexandre Landesmann<sup>1</sup>, Dinar Camotim<sup>2</sup>, Rafaela A. Garcia<sup>1</sup>

### **Abstract**

Results recently reported by Kumar & Kalyanaraman (2014) suggest that the presence of web and flange V-shaped intermediate stiffeners in cold-formed steel lipped channel columns may alter considerably their distortional buckling, post-buckling and collapse behaviors. The objective of this work is to assess the validity of this assertion, which constitutes a significant break from the existing knowledge, which is widely accepted by the technical/scientific community working with cold-formed steel structures. In particular, it may even imply that the application of the Direct Strength Method (DSM) to web/flange-stiffened lipped channel columns requires the consideration of a different (higher) distortional strength curve. In order to carry out the above assessment, this work reports a thorough numerical investigation aimed at assessing the peculiarities of the distortional buckling, post-buckling and collapse behaviors of (web/flange) stiffened cold-formed steel lipped channel columns. The first step consists of selecting column geometries associated with “pure” distortional buckling and failure modes, which is ensured by having local and global critical buckling loads much higher than their distortional counterparts – this task is carried out by means of sequences of “trial-and-error” buckling analyses, performed with the GBTUL code. Then, it is necessary to address the mechanical characterization of the distortional critical buckling modes in the stiffened columns, a task much more involved than in plain lipped channel columns (and by no means obvious). This is done through the in-depth inspection of the results provided by the aforementioned GBT buckling analyses. Next, an ANSYS shell finite element model is employed to perform geometrically and materially non-linear analyses of the selected stiffened lipped channel columns. The numerical results obtained (equilibrium paths, failure loads and deformed configurations) are then presented and discussed, in order to assess the influence of the V-shaped intermediate stiffeners. Finally, on the basis of the ultimate strength data obtained and also the experimental and numerical failure loads reported by Kumar & Kalyanaraman (2014), the paper presents some considerations concerning the application of the current DSM strength curve to the design of (web/flange) stiffened lipped channel columns failing in distortional modes – in particular, some conclusions are drawn concerning the need to develop a new DSM distortional design curve to handle columns with this cross-section shape.

### **1. Introduction**

Advances in the manufacturing process have prompted the cold-formed steel industry to search for novel cross-section shapes that, when compared with the most traditional ones, are structurally more efficient,

---

<sup>1</sup> Civil Eng. Progr., COPPE, Federal University of Rio de Janeiro, Brazil. <alandes@coc.ufrj.br>; <rafaelasanches@coc.ufrj.br>

<sup>2</sup> ICIST, CERis, DECivil, Instituto Superior Técnico, Universidade de Lisboa, Portugal. <dcamotim@civil.ist.utl.pt>

in the sense that they exhibit higher strength-to-weight ratios. The most common way of achieving this added efficiency is the inclusion of more or less complex end or intermediate stiffeners, a trend that was responsible for (i) the emergence of distortional failures, quite rare and very poorly understood three decades ago, and (ii) the inadequacy of the methods classically adopted to handle local failures, based on the widely accepted “effective width” concept – its application to more complex cross-section shapes involves cumbersome and time-consuming calculations. This situation provided the motivation for searching a novel unified design approach for cold-formed steel members capable of handling local and distortional (and also global) failures for arbitrarily complex cross-section shapes. This search led to the Direct Strength Method (DSM), which (i) has its roots in the work of Hancock *et al.* (1994), (ii) was originally proposed by Schafer & Peköz (1998) and (iii) mainly owes its progressive development, dissemination and firm establishment amongst the cold-formed steel technical/scientific community to the efforts of Schafer (2002, 2006, 2008), who can undoubtedly claim the “paternity” of the method. Because of its inherent simplicity and undeniable efficiency, the DSM rapidly became very popular, as attested by the fact that it has already been included in the current versions of the North American (AISI 2012), Australian/New Zealand (AS/NZS 2005) and Brazilian (ABNT 2010) specifications for cold-formed steel structures. The currently codified DSM provides design/strength curves/expressions to estimate the load-carrying capacity of columns failing in local, distortional, global and local-global interactive modes. These curves were calibrated and validated against numerical and experimental failure loads concerning almost exclusively columns with fixed-ended support conditions and exhibiting plain cross-section shapes, in the sense that they did contain intermediate stiffeners. It is worth noting that, at present, there are no codified DSM design curves capable of handling column (or beam, for that matter) exhibiting interactive failures involving distortional buckling/deformations. Indeed, the search for such design curves constitutes a topic of current research (*e.g.*, Dinis & Camotim 2015, for local-distortional interaction, Camotim & Dinis 2013, for distortional-global interaction, or Dinis *et al.* 2012, 2014, for local-distortional-global interaction) – it is worth mentioning that this goal is closer to achievement in the case of columns undergoing local-distortional interactive failures.

This work deals exclusively with the predictions yielded by the DSM distortional design curve, on the sole basis of the column critical distortional buckling stress and the steel yield stress, which means that the columns considered fail in pure distortional modes without any influence from either local or global buckling/deformations. Since this design curve was developed mostly in the context of fixed-ended columns with plain cross-sections, it is not surprising that its application to columns exhibiting other characteristics has raised some doubts. For instance, (i) an extensive parametric study carried out by Landesmann & Camotim (2013) showed that the current DSM distortional strength curve overestimates the failure loads of plain columns with other end support conditions and (ii) an experimental and numerical investigation reported by Kumar & Kalyanaraman (2014) suggested that this same curve considerably underestimates the failure loads of fixed-ended lipped channel columns with web and flange V-shaped intermediate stiffeners. The fact that the conclusions drawn by the authors of this last publication constitute a significant break from the existing knowledge, widely accepted by the technical/scientific community working with cold-formed steel structures, provided the motivation for the investigation whose results are reported in this paper. The objective of such investigation is to acquire in-depth knowledge concerning several aspects related to the structural response of web/flange-stiffened lipped channel columns (henceforth designated as “SLC columns”), namely (i) the buckling behavior and (ii) the “pure” distortional post-buckling and collapse behaviors (the use of the word “pure” means that there is no influence from either local or global buckling/deformations, which is ensured by selecting columns with local and global critical buckling loads significantly higher than their distortional counterparts). In

particular, it is intended to challenge the assertions made by Kumar & Kalyanaraman (2014), which, in the authors' opinion, are based on a number of erroneous assumptions – for instance, the authors believe that there is no need to develop new DSM distortional design curves for fixed-ended SLC columns.

Initially, the paper describes the column selection procedure, which aims at identifying SLC column geometries (cross-section dimensions and lengths) that ensure (i) buckling in pure distortional modes and (ii) local and global critical buckling loads significantly higher than their local counterparts). Because the distinction between “local” and “distortional” buckling is not straightforward in SLC columns is by no means straightforward (unlike in the plain lipped channel columns), the column selection procedure is preceded by the presentation and discussion of SLC column buckling results obtained through analyses based on Generalized Beam Theory (GBT), whose modal nature makes it possible to illustrate and clarify the meanings of the words “local” and “distortional” adopted in this work. Then, after describing and validating the ANSYS (SAS 2009) shell finite element non-linear model adopted, the paper addresses the “pure” distortional post-buckling (elastic and elastic-plastic) and collapse behaviors of the selected SLC columns, focusing on the influence of the V-shaped intermediate stiffeners. The numerical results presented and discussed comprise equilibrium paths, failure loads and deformed configurations, including collapse mechanisms. Finally, the failure loads gathered in this work, together with those reported by Kumar & Kalyanaraman (2014), are used to assess the merits of the current DSM distortional design curve, namely its suitability for SLC columns, challenged by these last authors.

## **2. Column Geometry Selection – Buckling Behavior**

The first stage of this work consisted of careful selecting the cross-section dimensions and lengths of the fixed-ended SLC columns to be analyzed. The selection procedure, which involved sequences of “trial-and-error” buckling analyses, (i) was performed using mostly code GBTUL (Bebiano *et al.* 2008a,b), but also ANSYS shell finite element models, and (ii) aimed at satisfying the following requirements:

- (i) Columns exhibiting “pure” distortional buckling and failure modes. This goal is achieved by ensuring that the critical buckling stress ( $i_1$ ) is clearly distortional and ( $i_2$ ) falls considerably below the lowest local and global bifurcation stresses.
- (ii) Cross-section dimensions commonly used in practice and, as much as possible, corresponding to distinct wall width proportions, namely web-to-flange and web-to-lip width ratios. This second requirement is intended to enable assessing whether such width proportions have a meaningful influence on the column distortional post-critical strength and failure load.
- (iii) Column lengths associated with single half-wave distortional buckling modes.

Before showing the fruits of this columns selection procedure, it is worth presenting and discussing some SLC column GBT-based buckling results, with the objective of clarifying the choices adopted in this work concerning the meaning of the words “local buckling” and “distortional buckling” – unlike in plain lipped channel (PLC) columns, the distinction is far from trivial. First of all, it should be said that it is commonly agreed that distortional deformations are associated with in-plane transverse displacements of cross-section internal corners (member fold lines). According to this definition, which was formulated having basically plain cross-sections in mind, and taking advantage of the GBT “modal language”, it can be said that PLC and SLC columns buckle in a “pure” distortional mode provided that the corresponding buckling mode shape exhibits a dominant contribution from one or more of the deformation modes depicted in Figures 1(a) (PLC) or 1(b) (SLC), which is often combined with a more or less minor contribution from the local deformation modes shown in Figures 2(a) (PLC) or 2(b) (SLC).

The comparative analysis of the PLC and SLC (cross-section) GBT deformation modes provided in Figures 1(a)-(b) and 2(a)-(b) prompts the following remarks:

- (i) First of all, the number of distortional deformation modes is significantly higher in the SLC, which is due to the additional number of internal corners stemming from the presence of the V-shaped intermediate stiffeners – note that the commonly accepted definition of distortional deformation mode is “*a mode involving in-plane transverse displacements of internal corners*”. While in the PLC there are only two distortional deformation modes (one symmetric and the other anti-symmetric), the SLC exhibits a total amount of 11 distortional deformation modes.
- (ii) Several SLC cross-section distortional deformation modes strongly resemble PLC local deformation modes (if the presence of the stiffeners is “ignored”). For instance, the shapes of the SLC and PLC deformation modes **7**, **8** and **9** depicted in Figs. 1(b) and (2(a)), are clearly similar – the only difference is the presence of “partially effective” stiffeners, in the sense that they are unable to prevent the in-plane transverse displacements of the web and flange mid-points.
- (iii) Although all the SLC “distortional” deformation modes displayed in Figs. 1(b) abide to the definition provided in item (i), an adequate structural assessment must treat them separately. For instance, the DSM distortional design curves aim at predicting ultimate strengths of members exhibiting collapse modes akin to combinations of deformation modes **5** and **6** – collapse modes involving dominant contributions from deformation modes **7** to **15** should be handled by DSM local design curves.
- (iv) In accordance to the content of the previous item, this work makes a clear distinction between the buckling behaviors involving deformations akin to modes **5+6** and **7-15** – note that Kumar & Kalyanaraman (2014) did not make this distinction.

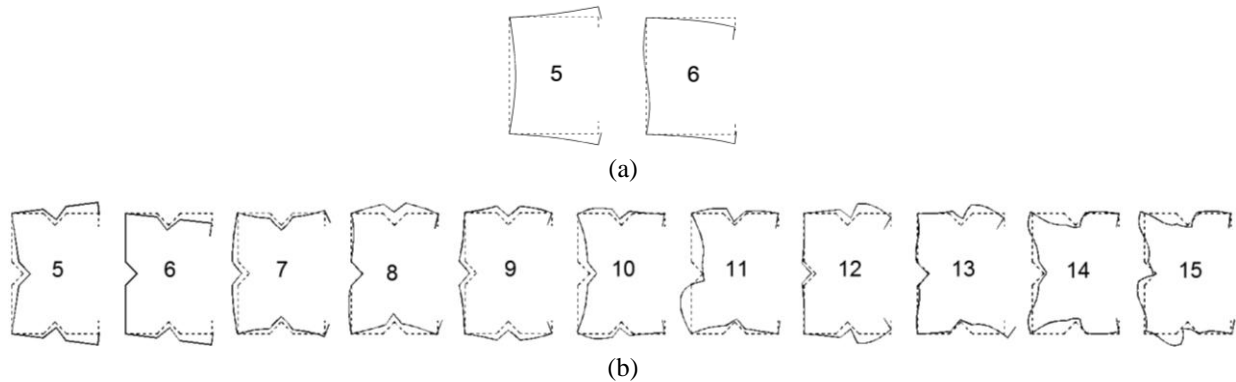


**Figure 1:** GBT distortional deformation modes of (a) plain and (b) stiffened lipped channel cross-sections.

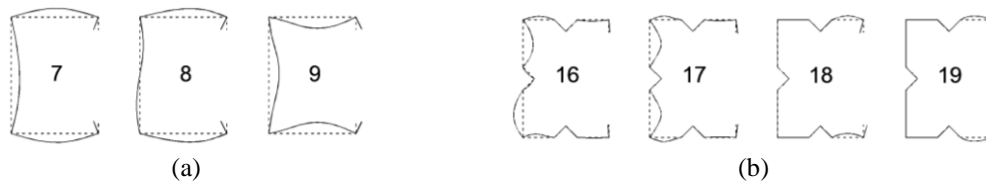


**Figure 2:** Most relevant GBT local deformation modes of (a) plain and (b) stiffened lipped channel cross-sections.

The end product of the “trial-and-error” selection procedure were the 23 SLC cross-section dimensions given in Table 1 and illustrated in Fig. 3(a) – Table 1 also provides the column cross-sectional areas and “distortional lengths”  $L_D$  (illustrated in Fig. 3(b)). It is worth noticing that (i) sections SLC-50-100-150 and SLC-120(1)-120(2)-120(3)-140-140(1) were previously analyzed by Kumar & Kalyanaraman (2014), either numerically (first set) or experimentally (second set), (ii) the web-to-flange width ratio

**Table 1:** SLC column cross-section dimensions, cross-sectional areas and lengths (see Fig. 3(b)).

SLC	$h$ (mm)	$b$ (mm)	$d$ (mm)	$t$ (mm)	$s_{Iw}$ (mm)	$s_{2w}$ (mm)	$s_{If}$ (mm)	$s_{2f}$ (mm)	$A$ (cm <sup>2</sup> )	$L_D$ (cm)
50	50	50	2.5	0.579	10	5	10	5	0.97	45
50(1)	50	50	4	0.579	10	5	10	5	0.99	45
50(2)	50	50	5.6	0.579	10	5	10	5	1.00	45
65	65	65	5	0.9	10	5	10	5	1.96	60
65(1)	65	65	7.5	0.9	10	5	10	5	2.00	60
65(2)	65	65	8.5	0.9	10	5	10	5	2.02	60
65(3)	65	65	4.33	0.9	10	5	10	5	1.95	50
75	75	75	7	1.2	12	6	12	6	3.05	60
75(1)	75	65	5	2	14	7	14	7	4.65	40
80	80	80	12	2	10	5	10	5	5.53	50
90	90	90	12	1.8	18	9	18	9	5.69	50
90(1)	90	90	7	1.8	18	9	18	9	5.51	50
90(2)	90	90	4.5	1.8	18	9	18	9	5.42	70
90(3)	90	90	9.5	1.8	18	9	18	9	5.60	70
100	100	100	5	1.2	15	7.5	15	7.5	3.94	80
100(1)	100	100	5	2.145	20	10	20	10	7.18	70
120	120	90	15	1.5	20	10	20	10	5.32	100
150	150	150	7.5	2.3	30	15	30	15	11.55	120
120(1)	1220	117.19	118.6	8.62	31.96	10.91	30.94	10.91	5.65	122
120(2)	1218	116.5	129.48	5.9	31.96	10.41	31.44	10.41	5.85	121.8
120(3)	1219	117.87	138.55	5.82	31.96	10.91	31.45	10.91	6.15	121.9
140	1218	136.29	128.56	8.72	31.44	10.41	31.96	10.91	6.20	121.8
140(1)	1220	137.7	138.37	4.41	31.96	10.91	30.94	10.41	6.37	122

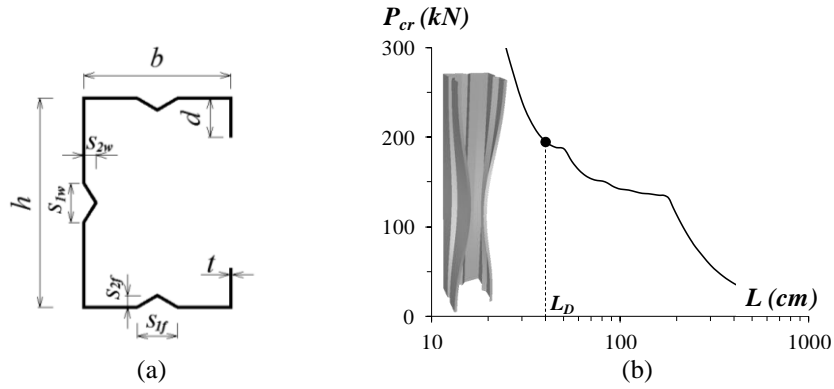


**Figure 3:** SLC column (a) cross-section dimensions and (b) illustrative  $P_{cr}$  vs.  $L$  curve indicating the selected length ( $L_D$ ) and showing the corresponding distortional buckling mode shape

( $h/b$ ) ranges from 0.85 to 1.33, (iii) the web-to-thickness ratio ( $h/t$ ) ranges from 37.5 to 95.6, (iv) the web-to-lip ratio ( $h/d$ ) ranges from 6.67 to 26.84, (v) the web intermediate stiffener width-to-depth ratio ( $s_{Iw}/s_{2w}$ ) varies from 2.0 to 2.6, (vi) the flange intermediate stiffener width-to-depth ratio ( $s_{If}/s_{2f}$ ) varies from 2.0 to 2.58, (vii) the web-to-stiffener width ratio ( $h/s_{Iw}$ ) varies from 3.7 to 8.0, and (viii) the flange-to-stiffener width ratio ( $b/s_{If}$ ) varies from 3.9 to 8.0. The SLC-50-100-150 columns considered in this

work are shorter than those analyzed by Kumar & Kalyanaraman (2014). It is worth mentioning that the SLC-50-100-150 columns considered in this work are a bit shorter than those analyzed by Kumar & Kalyanaraman (2014) – this length reduction was considered in order to obtain single half-wave distortional buckling and failure modes.

On the other hand, Table 2 provides, for the SLC columns with length  $L_D$ , (i) the critical (distortional) buckling loads  $P_{cr,D}$ , obtained by means of GBT buckling analyses including all deformation modes<sup>3</sup>, and (ii) the ratios between the lowest local ( $P_{b1,L}$ ) and global ( $P_{b1,G}$ ) bifurcation loads and  $P_{cr,D}$ , where the values of  $P_{b1,L}$  and  $P_{b1,G}$  are obtained by means of GBT buckling analyses including only local and global deformation modes, respectively – note that ratios  $P_{b1,L7}/P_{cr,D}$  are also given, where  $P_{b1,L7}$  are bifurcation loads obtained by means of GBT buckling analyses including deformation modes of order higher than 6 (*i.e.*, excluding only the global and “truly distortional” modes). This table also gives the Young’s modulus values considered to obtain the buckling/bifurcation loads – the Poisson’s ratio adopted was always  $\nu=0.3$ .

**Table 2:** SLC and PLC column critical (distortional) buckling loads and local/global buckling load ratios.

SLC	$E$ (GPa)	$\frac{P_{b1,L7}}{P_{cr,D}}$	$\frac{P_{b1,L}}{P_{cr,D}}$	$\frac{P_{b1,G}}{P_{cr,D}}$
50	202	2.93	7.65	17.3
50(1)	202	5.44	6.45	15.1
50(2)	202	4.46	4.96	12.22
65	210	5.32	8.78	15.1
65(1)	210	3.66	6.44	11.77
65(2)	210	3.07	5.63	10.54
65(3)	210	5.52	8.95	22.52
75	210	4.74	8.34	14.8
75(1)	210	4.18	11.73	13.7
80	210	2.02	7.65	10.2
90	210	3.11	4.97	11.6
90(1)	210	4.87	8.61	18.4
90(2)	210	3.02	12.11	12.6
90(3)	210	5.12	9.18	10.26
100	200	4.62	9.00	27.7
100(1)	202	3.06	12.69	14.1
120	200	2.80	3.85	8.95
150	202	2.97	9.54	16
120(1)	202	5.55	9.83	11.7
120(2)	202	3.37	10.51	15.5
120(3)	202	3.23	9.41	17.53
140	202	5.12	7.73	18.6
140(1)	202	2.38	9.82	26.4

The analysis of the results presented in Table 3 shows that, as intended, all the columns analyzed in this work (i) buckle in critical distortional modes and (ii) have their first “non-distortional” bifurcation

<sup>3</sup> The buckling modes are not “purely distortional”, as they exhibit more or less small contributions from deformation modes of order higher than 6 – mainly modes 7 and 9, which are here “treated as local”.

loads well above  $P_{cr,D}$ . Such bifurcation loads are always “local”, in the sense that they correspond to buckling modes exhibiting only contributions from deformations modes of order higher than 6 (the first global bifurcation loads are always much higher). Quantitatively speaking, the values of the ratios  $P_{b1,L7}/P_{cr,D}$  and  $P_{b1,L}/P_{b1,L7}$  are inside the intervals 2.02-5.55 and 3.85-12.69, respectively.

### 3. Column Post-Buckling Analysis

#### 3.1 Numerical Model

The column distortional post-buckling equilibrium paths and ultimate strength values were determined through geometrically and materially non-linear SFEA carried out in the code ANSYS (2009). The columns were discretized into *SHELL181* elements (ANSYS nomenclature: 4-node shear deformable thin-shell elements with six degrees of freedom per node and full integration) – convergence studies showed that  $5\text{ mm} \times 5\text{ mm}$  meshes provide accurate results, while involving a reasonable computational effort (Garcia *et al.* 2014). The analyses were performed by means of an incremental-iterative technique combining Newton-Raphson’s method with an arc-length control strategy. All columns (i) contained critical-mode (distortional) initial imperfections with fairly small amplitudes (given as percentages of the wall thickness  $t$ ) and (ii) exhibited a material behavior either elastic or elastic-perfectly plastic (Prandtl-Reuss model: von Mises yield criterion and associated flow rule), characterized by  $E=200\text{-}210\text{ GPa}$  (see Table 3),  $\nu=0.3$  and several yield stresses  $f_y^4$ . It should be noted that no strain-hardening, residual stresses and/or rounded corner effects were considered in the analyses.

The incorporation of the critical-mode initial geometrical imperfections in the columns was made automatically by means of the procedure described by Landesmann & Camotim (2013), which involves the following steps: (i) determination of the critical buckling mode shape (through ANSYS SFE buckling analysis adopting the column discretization subsequently employed to perform the post-buckling analysis), (ii) scaling of this buckling mode so that the exhibit maximum vertical displacements along the flange-lip longitudinal edges is equal to  $0.1 t$  and (iii) use this buckling analysis output as input of the post-buckling (non-linear) one. Following the findings of Silvestre & Camotim (2006), concerning the distortional post-buckling asymmetry of SLC columns, these initial imperfections involve inward flange-lip motions – those shown to lead to the lower post-buckling strengths.

Concerning the modeling of the end support conditions, the column end cross-sections were attached to rigid plates, thus precluding the occurrence of warping and local and global displacements and rotations. Moreover, in order to enable the load application, the rigid-body axial translation is free at either one or both end cross-sections – in the latter case, the axial translation of one mid-section point is prevented. The axial compression is applied by means of a concentrated force applied on the rigid plate point(s) corresponding to end cross-section centroid. The force application is made in small increments, taking advantage of the ANSYS automatic “load stepping procedure”.

#### 3.2 Validation Studies

In order to validate the use of the ANSYS shell finite element model just described to assess the distortional post-buckling behavior and strength of cold-formed steel columns, one compares next the post-buckling

---

<sup>4</sup> Several yield stresses considered in this work are unrealistically high, corresponding to  $E/f_y$  values as low 60, *i.e.*, largely below the 340 limit value currently prescribed by the AISI specification (2012) for the application of the DSM – pre-qualified columns. Such high yield stresses were selected to enable the analysis of columns with high slenderness values, thus making it possible to cover a wide (distortional) slenderness range.

results obtained with this model with the experimental values reported by Kumar & Kalyanaraman (2014) and concerning the tests of 14 fixed-ended SLC columns designed to buckle and fail in distortional modes. Moreover, since one of the main objectives of this work is to challenge the findings of the above authors, the results of the numerical simulations, involving those same columns, carried out by them (adopting very questionable support conditions, which will be addressed in some detail later) are also compared with the numerical values obtained in this work. Figures 4(a)-(b) provide an overall view of the experimental test set-up and finite element model used by Kumar & Kalyanaraman (2014).

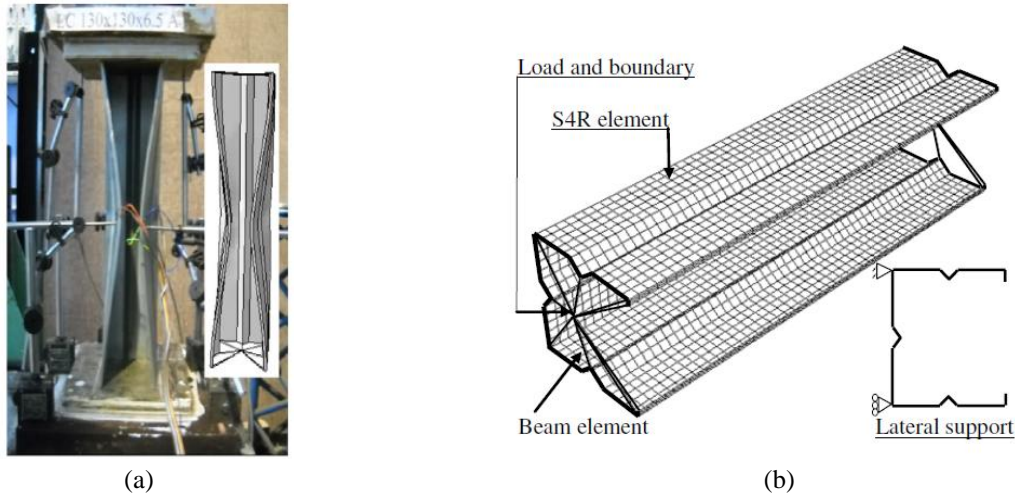


**Figure 4:** (a) Experimental test set-up and (b) finite element model used by Kumar & Kalyanaraman (2014).

The comparison between (i) the experimental and numerical results that were recently reported by Kumar & Kalyanaraman (2014) and (ii) the numerical values obtained in this work concerns four columns, namely SLC-120(1)-120(2)-120(3)-140-140(1) (see Tables 1 and 2). Figures 5(a)-(b) compare, for the columns SLC 120(3)-140(1), the experimental and numerical equilibrium paths relating the applied load ( $P$ ) to the (i) transverse/vertical (normal to the flange) displacements of the flange-lip corner of the cross-section located 200 mm away from the column mid-height (bottom half)<sup>5</sup> ( $\delta$ ) and (ii) the column axial shortening ( $\Delta$ ). Each plot displays three equilibrium paths, corresponding to (i) the experimental ( $P_{KK.exp}$ ) and numerical ( $P_{KK.num}$ ) results of Kumar & Kalyanaraman (2014), and (ii) the numerical results obtained in this work ( $P_{TW.num}$ ). Note that all numerical results concern columns with the yield stresses given in Table 4 and containing critical-mode initial geometrical imperfections with amplitude  $0.94t$  (as adopted by Kumar & Kalyanaraman). Moreover, the numerical results of Kumar & Kalyanaraman concern laterally restrained columns (see Fig. 5(b)), unlike the experimental ones and those obtained in this work.

On the other hand, Table 3 provides, for the columns SLC-120(1)-120(2)-120(3)-140-140(1), the failure load values (i) reported by Kumar & Kalyanaraman (2014) ( $P_{u.KK.exp}$  and  $P_{u.KK.num}$ ) and (ii) obtained in this work for laterally restrained ( $P_{u.TW.num.R}$ ) and free ( $P_{u.TW.num.F}$ ) columns. Also shown are the column yield stresses and values of the  $P_{u.TW.num.F}/P_{u.KK.exp}$  and  $P_{u.TW.num.R}/P_{u.KK.num}$  ratios.

The observation of the results displayed in Figs. 5(a)-(b) and Table 3 leads to the following conclusions:

- (i) The numerical results obtained in this work for laterally free columns are in fairly good agreement with the experimental values reported by Kumar & Kalyanaraman (2014). Indeed, (i<sub>1</sub>) it is clear that the numerical equilibrium paths obtained in this work follow quite closely the experimental ones and

<sup>5</sup> Location of the experimental/numerical transverse displacements reported/plotted by Kumar & Kalyanaraman (2014).

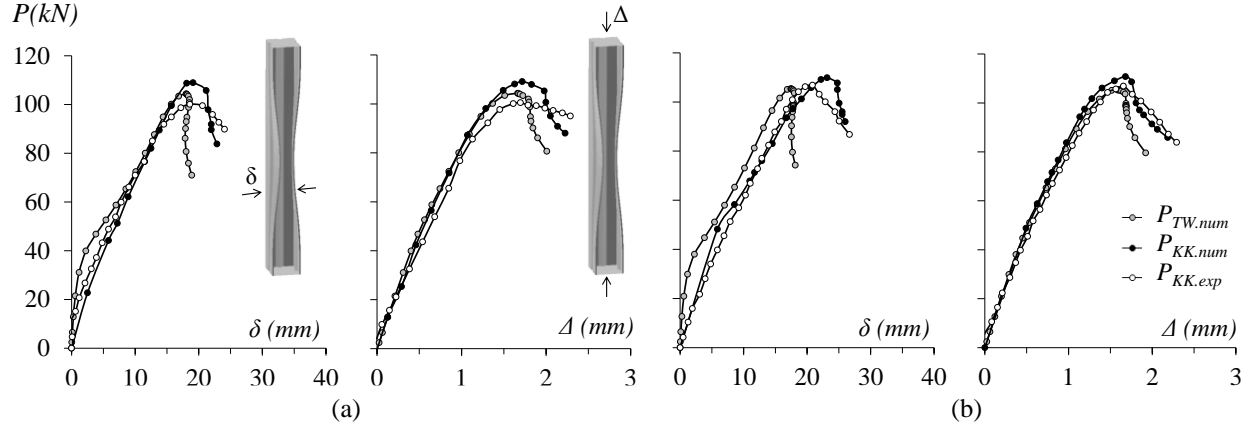


**Figure 5:** Experimental and numerical (a) SLC 120(3) and (b) SLC 140(1) column  $P$  vs.  $\delta$  and  $P$  vs.  $\Delta$  equilibrium paths.

**Table 3:** Failure loads reported by Kumar & Kalyanaraman (2014) and obtained in this work.

$SLC$	$f_y$ (MPa)	$P_{u.KK.exp}$ (kN)	$P_{u.TW.num.F}$ (kN)	$P_{u.KK.num}$ (kN)	$P_{u.TW.num.R}$ (kN)	$\frac{P_{u.TW.num.F}}{P_{u.KK.exp}}$	$\frac{P_{u.TW.num.R}}{P_{u.KK.num}}$
120(1)	285	101.9	101.9	108.8	103.6	1.000	0.952
120(2)	284	104.5	100.6	106.3	102.6	0.963	0.965
120(3)	283	100.5	104.4	108.7	106.0	1.039	0.975
140	285	104.0	106.1	110.5	109.3	1.020	0.989
140(1)	285	106.9	105.5	110.6	108.0	0.987	0.976

(i<sub>2</sub>) the corresponding failure loads correlate rather well – the  $P_{u.TW.num.F}/P_{u.KK.exp}$  values are comprised between 0.963 and 1.039.

- (ii) The numerical failure loads obtained in this work for laterally restrained columns also agree fairly well with those reported by Kumar & Kalyanaraman (2014), even if all the  $P_{u.TW.num.R}/P_{u.KK.num}$  values are slightly below 1.00 – they are comprised between 0.952 and 0.989.
- (iii) On the basis of the comparisons made in the previous items, it seems fair argue that the shell finite element model employed in this work may be deemed as adequately validated.
- (iv) It is interesting to notice that all numerical failure loads obtained for the restrained columns, either in this work or by Kumar & Kalyanaraman, overestimate the experimental values. This overestimation is more pronounced in the latter case, as the values of the ratio  $P_{u.KK.num}/P_{u.KK.exp}$  are comprised between 1.017 and 1.082. In the authors' opinion, the decision to perform numerical simulations of the experimental tests, in which the specimens were laterally free, using a model with the column laterally restrained (displacements associated with minor-axis flexure prevented) is questionable – this issue will be further addressed in the next Section.

#### 4. Critical Analysis of the Results Reported by Kumar & Kalyanaraman (2014)

Kumar & Kalyanaraman (2014) reported experimental and numerical results concerning fixed-ended SLC columns and, on the basis of these results, proposed a new DSM distortional strength curve for the design of such columns – it should be mentioned that the proposed design curve (i) lies well above the currently codified (AISI 2012) DSM distortional design curve, which is supposedly applicable to predict

the distortional failures of columns with any cross-section shape and, quite surprisingly, (ii) lies also above the currently codified DSM *local* design curve<sup>6</sup>. The fact that the proposed DSM distortional strength curve is based on findings that constitute a significant break from the existing knowledge, widely accepted by the technical/scientific community working with cold-formed steel structures, led the authors of this paper to investigate this subject further.

The experimental results of Kumar & Kalyanaraman (2014) concern 14 fixed-ended SLC columns failing in distortional modes and exhibiting (i) web-to-lip width ratios comprised between 12 and 27 ( $h/d > 18$  for most columns) and (ii) small-to-moderate distortional slenderness values, comprised between 1.15 and 1.81. Moreover, these authors reported results of ABAQUS numerical (SFE) analyses also concerning SLC columns. All the columns analyzed incorporated critical-mode (distortional) initial geometrical imperfections with amplitude equal to  $0.94t$  and involving inward flange-lip motions – no residual stress and corner strength effects were considered. With the stated objective of “precluding overall buckling”, the SFE model employed had the rigid-body in-plane translations and torsional rotations prevented along the whole column length – this was achieved by means of continuous horizontal supports located along the columns web-flange longitudinal edges, as illustrated Fig. 4(b)). The SFEA were used (i) to simulate the columns column tests reported previously and (ii) to perform a parametric study intended to generate additional distortional ultimate strength data. This parametric study consisted of 12 fixed-ended SLC columns with (i) a constant web-to-lip width ratio ( $h/d=20$ ) and (ii) distortional slenderness comprised between 1.00 and 1.75. Finally, on the basis of the obtained column distortional failure load data bank (14 experimental values and 12 numerical ones), Kumar & Kalyanaraman (2014) (i) concluded that the currently codified DSM distortional strength curve provided excessively safe failure load estimates for SLC columns and, consequently, (ii) proposed an alternative (more “liberal”) DSM design curve specifically intended to predict distortional failures of SLC columns.

After studying closely the work reported by Kumar & Kalyanaraman (2014), the authors were able to identify a number of questionable issues that are bound to influence, to a smaller or larger extent, the conclusions drawn in the above paper – in particular, the need to use specific DSM design curve for the design of SLC columns against distortional failure. These issues are briefly summarized next (their implications are addressed afterwards):

- (i) The authors fail to see the need to perform numerical analyses of columns with the rigid-body in-plane translations and torsional rotations prevented along the whole length, since these additional support conditions are not present in the experimental tests reported (and rightful so) and seldom occur in practice. The aim of ensuring “pure” distortional deformations up to the failure load does not seem appropriate, particularly because it unduly eliminates the minor-axis bending caused by a possible effective centroid horizontal (normal to the web) shift, which should not be artificially removed from the column distortional post-buckling behavior. Naturally, these additional support conditions render the columns stiffer and, therefore, increase their failure loads – recall that all the experimental failure loads reported by Kumar & Kalyanaraman (2014) were overestimated by the corresponding numerical simulations (a few illustrative examples were presented in Section 3).

---

<sup>6</sup> However, it should be mentioned that these authors had previously proposed a new DSM local strength curve for SLC columns (Kumar & Kalyanaraman 2012). Nevertheless, these authors (Kumar & Kalyanaraman 2014) state explicitly that “*The post-distortional buckling strength (of the SLC columns) can be greater than the post-local buckling strength of the lipped channel (PLC) columns section, having the same value of the respective nondimensional slenderness ratios, particularly for sections having smaller values of  $h/b$* ”.

- (ii) The columns analyzed, experimentally or numerically, cover a quite limited (small-to-moderate) distortional slenderness range, comprised between  $1.00$  and  $1.81$ .
- (iii) The numerical results presented concern  $12$  columns, all exhibiting the same web-to-lip width ratio ( $h/d=20$ ). Even if the experimental failure loads correspond to columns with  $h/d$  comprised between  $12$  and  $27$ , a relevant range is not adequately covered.
- (iv) The decision to propose of a new DSM distortional design curve specifically for SLC columns, on the sole basis of just  $14$  experimental and  $12$  numerical failure loads, seems clearly premature, particularly since the new design curve lies well above the existing one.

Concerning the use of the additional support conditions in the numerical analyses, Figs. 6(a)-(b) display the equilibrium paths  $P/P_{cr,D}$  vs.  $|\delta|/t$  concerning columns SLC 140(1) and SLC 120(3), both simulating experimental tests (see Table 1), with the rigid-body in-plane translations and torsional rotations either free or fully prevented. It is observed that, as was also mentioned by Kumar & Kalyanaraman (2014), the two pairs of equilibrium paths only differ in the fairly close vicinity of the failure load. Nevertheless, it is clear that the additional support conditions increase the column distortional failure loads – recall that Kumar & Kalyanaraman reported that their numerical simulations overestimated the experimental distortional failure loads by an amount varying between  $1.6\%$  and  $12.2\%$ <sup>7</sup>. It is still worth noting that the additional support conditions have a slightly larger influence on the distortional post-buckling behavior of plain lipped channel columns, as shown in Fig. 7 for a column analyzed by Santos et al. (2014) – note that the restrained column equilibrium path is always visibly (but marginally) above its free column counterpart.

In order to complement the failure load set considered by Kumar & Kalyanaraman (2014) and overcome its aforementioned limitations, the next Section includes a numerical (ABAQUS SFEA) parametric study involving  $155$  SLC columns and aimed at obtaining a more representative distortional failure load data bank – in particular, the columns analyzed exhibit (i) web-to-lip width ratios ranging from  $6.67$  to  $26.84$  and (ii) distortional slenderness values varying between  $0.62$  to  $3.69$ . Then, the extended SLC distortional failure load set, comprising the numerical values obtained in this work and the experimental and numerical values reported by Kumar & Kalyanaraman, is used to assess the merits of the DSM distortional strength curve newly proposed by these authors. In order to enable a visualization of how

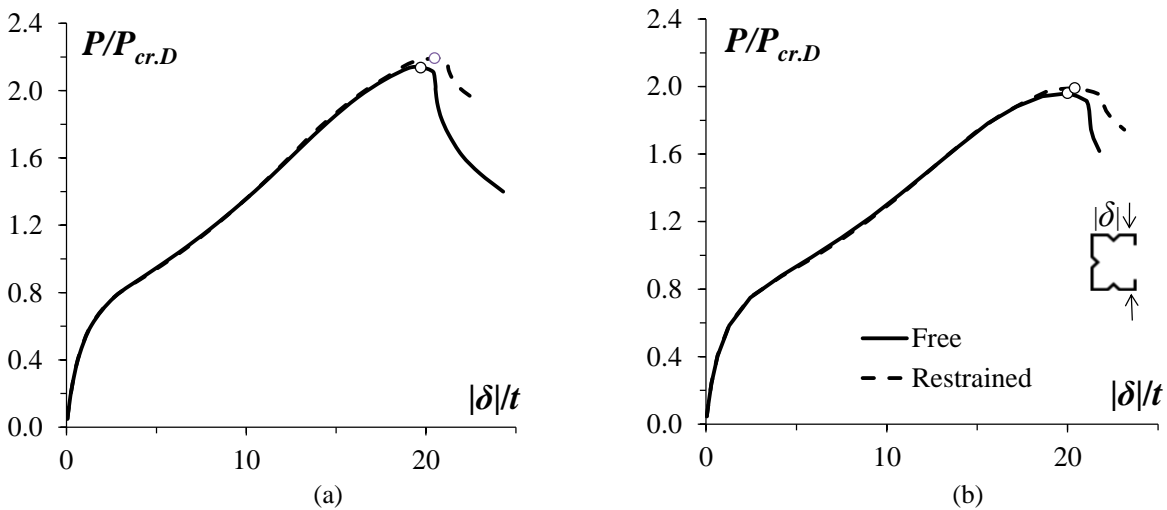


**Figure 6:** Equilibrium paths of (a) SLC 140(1) and (b) SLC 120(3) columns with and without the additional support conditions.

<sup>7</sup> The numerical simulations performed by the authors showed differences comprised between  $1.3\%$  and  $3.9\%$  (see Table 4).

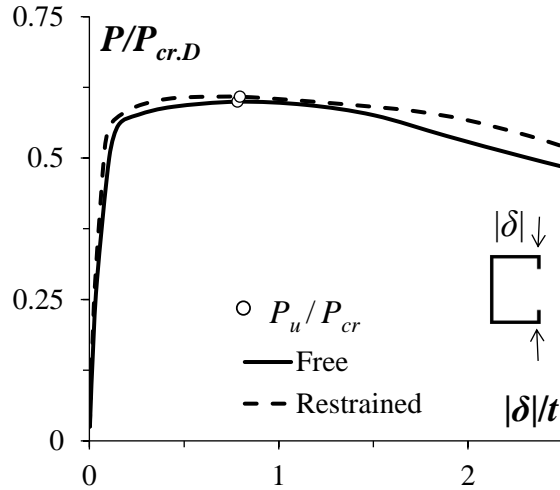


**Figure 7:** Equilibrium paths of plain lipped channel columns with and without the additional support conditions.

“revolutionary” this strength curve, Fig. 8 shows a comparison between (i) the currently codified DSM local ( $P_u/P_y$  vs.  $\lambda_L$  – DSM-L) and distortional ( $P_u/P_y$  vs.  $\lambda_D$  – DSM-D) design curves, and (ii) the proposed distortional strength curve ( $P_u/P_y$  vs.  $\lambda_D$  – DSM-DP). It is observed that:

- (i) Except for quite stocky columns, the DSM-DP curve always lies above its DSM-D counterpart. Moreover, the differences quickly become quite large and keep growing as  $\lambda_D$  increases – recall the Kumar & Kalyanaraman (2014) did not analyze any SLC column with  $\lambda_D$  higher than 1.81.
- (ii) For slenderness values higher than about 1.5, the DSM-DP curve even lies above the DSM-L one, which is really surprising, in view of the well-known fact that the column local post-critical strength reserve significantly exceeds its local counterpart<sup>8</sup>.

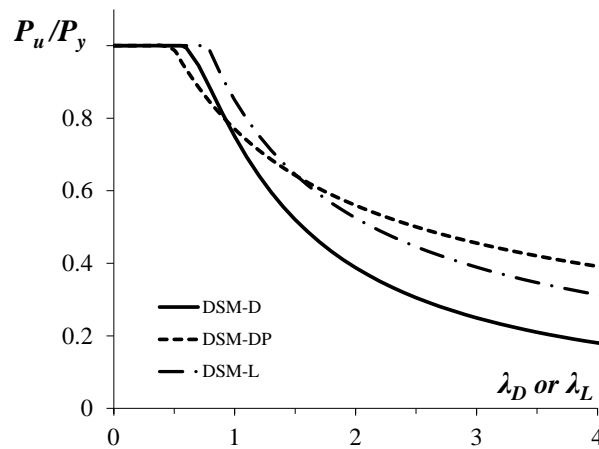


**Figure 8:** Comparison between the distortional strength curve proposed by Kumar & Kalyanaraman (2014) and the currently codified DSM local and distortional design curves.

<sup>8</sup> Apparently, Kumar & Kalyanaraman (2012) “solved” this discrepancy by proposing a new DSM local strength curve for SLC columns that lies above the DSM-L curve. It is beyond the scope of this work to challenge this other surprising strength curve proposed by the same authors.

## 5. Parametric Study – Column Elastic-Plastic Post-Buckling and Ultimate Strength Behavior

The ANSYS shell finite element model described and validated in Section 3 is now employed to perform a parametric study aimed at assessing the elastic-plastic post-buckling and ultimate strength behaviors of SLC columns buckling and failing in distortional modes. The numerical results presented and discussed concern a total of 155 columns, corresponding to all the combinations of (i) the 23 column geometries and material properties defined in Tables 1 and 2 and (ii) several yield stresses, selected to enable covering wide distortional slenderness ranges for all column sets:  $\lambda_D$  varies from 0.62 to 3.69 – recall that  $\lambda_D = [P_y/P_{cr,D}]^{0.5}$ , where  $P_y = A \cdot f_y$  and  $A$  is the cross-section area. Tables A1 to A4, included in Annex A, provide the SLC column (i) yield stresses  $f_y$ , (ii) squash loads  $P_y$ , (iii)  $\lambda_D$  values, (iv) failure loads  $P_u$  and associated limit  $|\delta|/t$  values, denoted  $(|\delta|/t)_{lim}$ , and (v) ultimate load ratios  $P_u/P_{cr,D}$  and  $P_u/P_y$ .

Figure 9 illustrates the non-linear equilibrium paths  $P/P_{cr,D}$  vs.  $|\delta|/t$  determined to obtain the distortional failure loads  $P_u$  (identified by white circles) – these equilibrium paths concern SLC 120 column with yield stresses  $f_y = 250-550-750-1200 \text{ MPa}$  (the elastic equilibrium path is also presented for comparative purposes). Moreover, the evolution of the  $f_y = 750 \text{ MPa}$  column deformed configurations and von Mises stress contours (before, at and beyond the peak load) is also depicted – the 4 diagrams correspond to the equilibrium states I-II-III-IV indicated on the equilibrium path (black and white circles). It is worth noting that (i) the deformed configurations are amplified 3 times, and (ii) state II corresponds to the column collapse (the failure mode is shown). The observation of these results prompts the following remarks:

- (i) The column exhibit single half-wave distortional buckling and failure modes with inward mid-span flange-lip motions.
- (ii) Yielding starts at mid-span zone – see diagram I. Collapse is associated with the full yielding of the web-flange junction and also the web-lip junction mid-span region, leading to the formation of a “distortional plastic hinge” – see diagram II, which also reveals that plasticity has already spread throughout almost the whole column length.

Figures 10(a)-(b) provide the failure load ratios  $P_u/P_{cr,D}$  (Fig. 10(a)) and  $P_u/P_y$  (Fig. 10(b)) against the distortional slenderness  $\lambda_D$  for the SLC columns (i) tested by Kumar & Kalyanaraman (2014) ( $P_{u,KK,exp}$ ), (ii) numerically analyzed by these authors ( $P_{u,KK,num}$ ) and (iii) numerically analyzed in this work ( $P_u$ ). In order to assess the influence of the web-to-lip width ratio  $h/d$ , the  $P_u/P_{cr,D}$  and  $P_u/P_y$

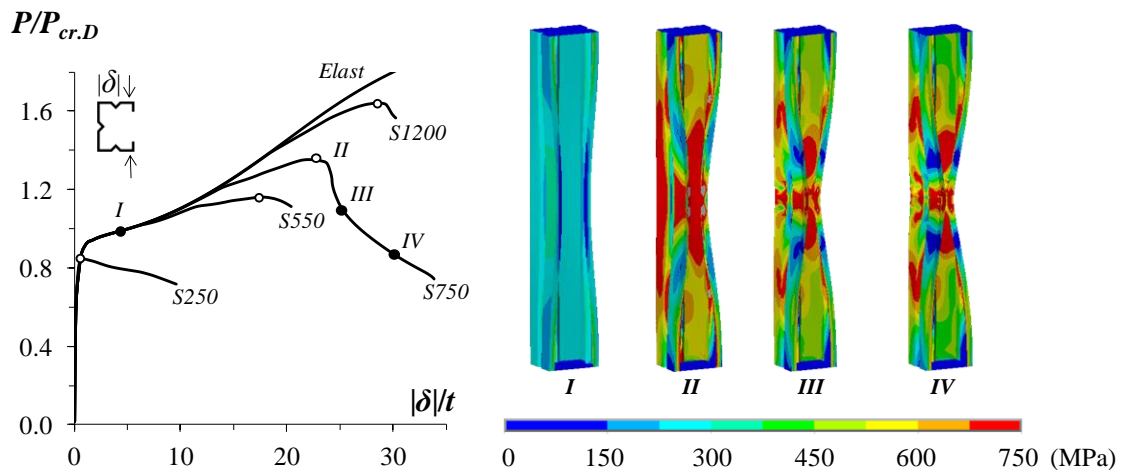


**Figure 9:** Distortional elastic-plastic equilibrium paths ( $P/P_{cr,D}$  vs.  $|\delta|/t$ ), deformed configurations and von Mises stress contours concerning the SLC 120 column with  $f_y = 750 \text{ MPa}$ .

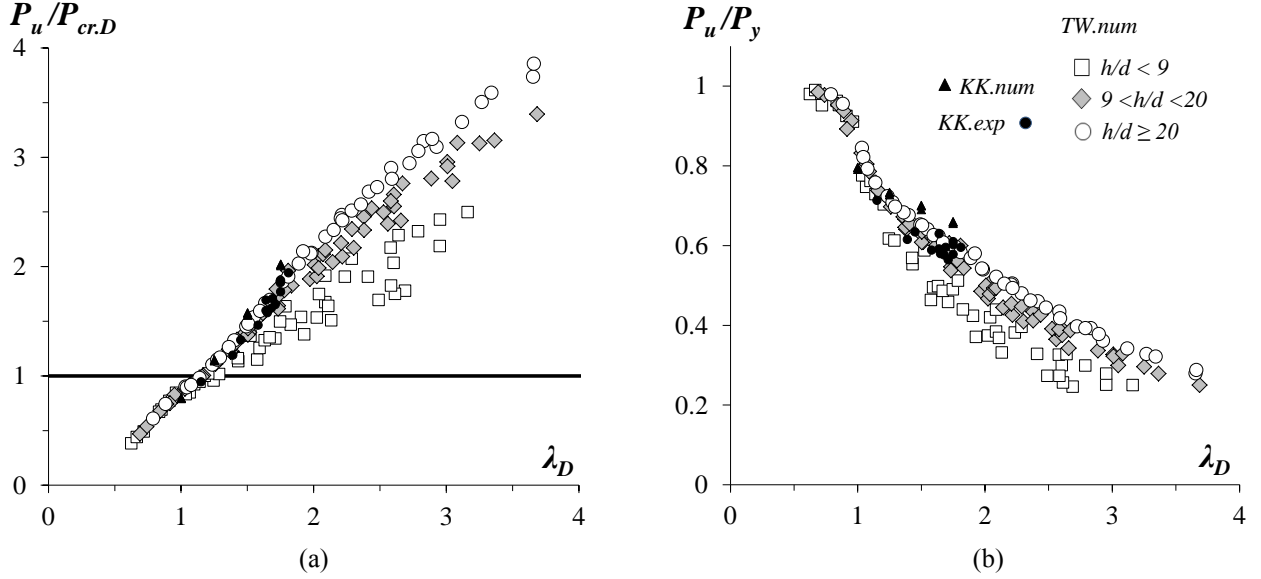


**Figure 10:** Plots of the ultimate load ratios (a)  $P_u/P_{cr,D}$  and (b)  $P_u/P_y$  against the distortional slenderness  $\lambda_D$ .

values obtained in this work are identified by (i) white circles, for  $h/d \geq 20$ , (ii) grey diamonds, for  $9 < h/d < 20$ , and (iii) white squares, for  $h/d < 9$ . Recall that the values reported by Kumar & Kalyanaraman concern columns with  $h/d$  values comprised between 12 and 27 ( $h/d=20$  for all the numerical ones) – they are identified by black triangles (numerical) and circles (experimental). The observation of the results shown in Figs. 10(a)-(b), as well as the data given in Tables A1 to A4, leads to the following conclusions:

- (i) Figure 10(a) shows that, naturally, the failure load ratios  $P_u/P_{cr,D}$  of the SLC columns analyzed (in this work and by Kumar & Kalyanaraman) increase with the distortional slenderness  $\lambda_D$  – note that  $P_u/P_{cr,D} > 1$  for  $\lambda_D$  larger than approximately 1.1. The variation  $P_u/P_{cr,D}$  vs.  $\lambda_D$  is fairly linear and, for  $\lambda_D > 1.5$ , it is noticeable that the slope increases with  $h/d$  – in particular, the values concerning the columns with  $h/d < 9$  visibly and consistently deviate (“down”) from the remaining ones.
- (ii) As expected, the  $P_u/P_y$  vs.  $\lambda_D$  “cloud” depicted in Fig. 10(b) follows the general trend of a “Winter-type” strength/design curve. However, a considerably  $P_u/P_y$  “vertical dispersion” is observed, particularly in the high slenderness range – indeed, the  $P_u/P_y$  values only exhibit a small vertical dispersion for  $\lambda_D$  lower than about 1.25. Moreover, like for the  $P_u/P_{cr,D}$  ratios, there is again a very clear influence of  $h/d$  on the  $P_u/P_y$  values. Indeed, this geometric ratio is the main “culprit” for the aforementioned vertical dispersion – for a given (high)  $\lambda_D$  value,  $P_u/P_y$  clearly decreases with  $h/d$ .
- (iii) It is very clear that the set of experimental and numerical (mostly) results reported by Kumar & Kalyanaraman is insufficient to draw meaningful conclusions concerning the DSM design of SLC columns failing in distortional modes. In fact, as already mentioned, they (iii<sub>1</sub>) cover only the 1.00-1.81 slenderness interval and (iii<sub>2</sub>) exhibit mostly  $h/d$  ratios either in close vicinity or above 20 (the value shared by all the columns analyzed numerically).
- (iv) In the next Section, the failure load data bank presented and discussed here is used to assess the DSM design of SLC columns against distortional failures.

## 6. DSM Design Considerations

The adequacy of the currently codified DSM distortional design curve, termed here DSM-D and defined by the expressions

$$P_{n,D} = \begin{cases} P_y & \text{for } \lambda_D \leq 0.561 \\ P_y \left[ 1 - 0.25 \left( P_{cr,D} / P_y \right)^{0.6} \right] \left( P_{cr,D} / P_y \right)^{0.6} & \text{for } \lambda_D > 0.561 \end{cases}, \quad (1)$$

to estimate SLC column failure loads is now addressed, devoting particular attention to the comparison between its predictions and those provided by the alternative strength curve recently proposed by Kumar & Kalyanaraman (2014) – the DSM-DP curve, defined by

$$P_{n,DP} = \begin{cases} P_y & \text{for } \lambda_D \leq 0.474 \\ P_y \left[ 1 - 0.23 \left( P_{cr,D} / P_y \right)^{0.3} \right] \left( P_{cr,D} / P_y \right)^{0.3} & \text{for } \lambda_D > 0.474 \end{cases}. \quad (2)$$

Note that the two design curves, which were already displayed in Fig. 9, exhibit the same format and only differ in the three coefficients.

Figures 11(a)-(b) compares the both the DSM-D and DSM-DP strength curves with the failure load ratios  $P_u/P_y$  concerning the SLC columns (i) experimentally ( $P_{u, KK.exp}$ ) and numerically ( $P_{u, KK.num}$ ) analyzed and by Kumar & Kalyanaraman (Fig. 11(a)) and (ii) numerically analyzed in this work (Fig. 11(b)) – the latter are separated according to their  $h/d$  ratios. On the other hand, Figs. 12(a)-(b) plot those same  $P_u/P_{n,D}$  and  $P_u/P_{n,DP}$  ratios against  $\lambda_D$ , thus providing pictorial representations of the accuracy and safety associated with the two design curves under consideration – the averages, standard deviations and maximum/minimum values of the  $P_u/P_{n,D}$  or  $P_u/P_{n,DP}$  ratios included in each plot are also given. The analysis of the design results presented in the above two figures leads to the following comments:

- (i) First of all, the observation of Figs. 11(a) and 12(a<sub>1</sub>) provides very clear evidence on why Kumar & Kalyanaraman (2014) proposed the DSM-DP design curve: it fits their 26 experimental and numerical failure loads almost perfectly!<sup>9</sup> Indeed, the corresponding indicators are 1.02 (average),

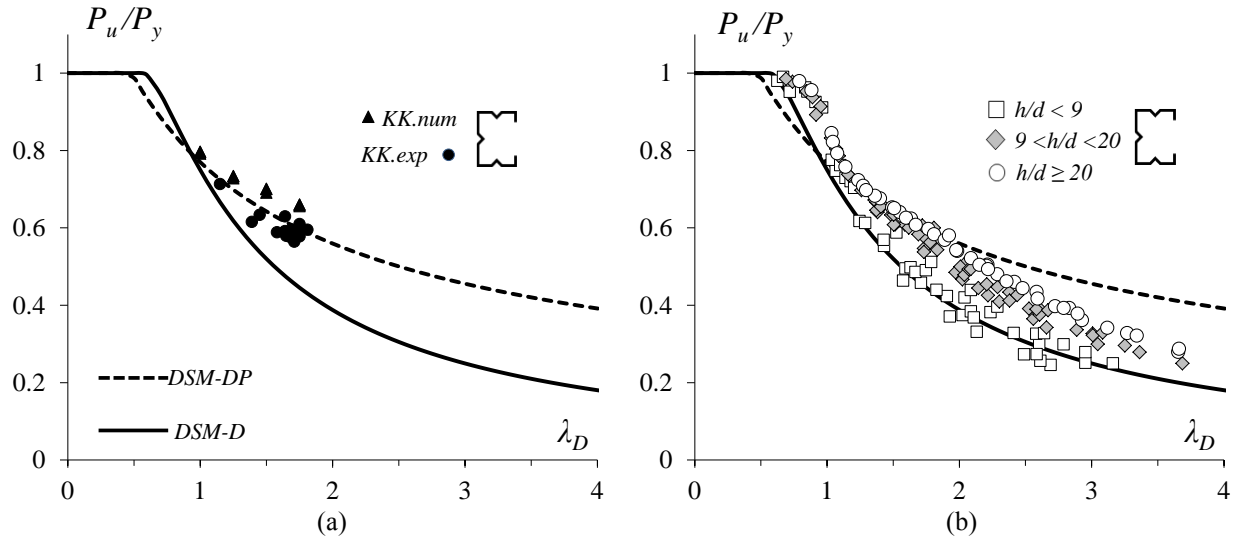


**Figure 11:** Comparison between the DSM-D and DSM-DP strength curves and the SLC column failure loads obtained (a) by Kumar & Kalyanaraman (2014) and (b) in this work.

<sup>9</sup> Recall that their numerical failure loads were obtained for laterally restrained SLC columns – even if it was shown that the restraints do not influence significantly the SLC column failure load, the removal of such restraints would necessarily decrease them by a few percent.

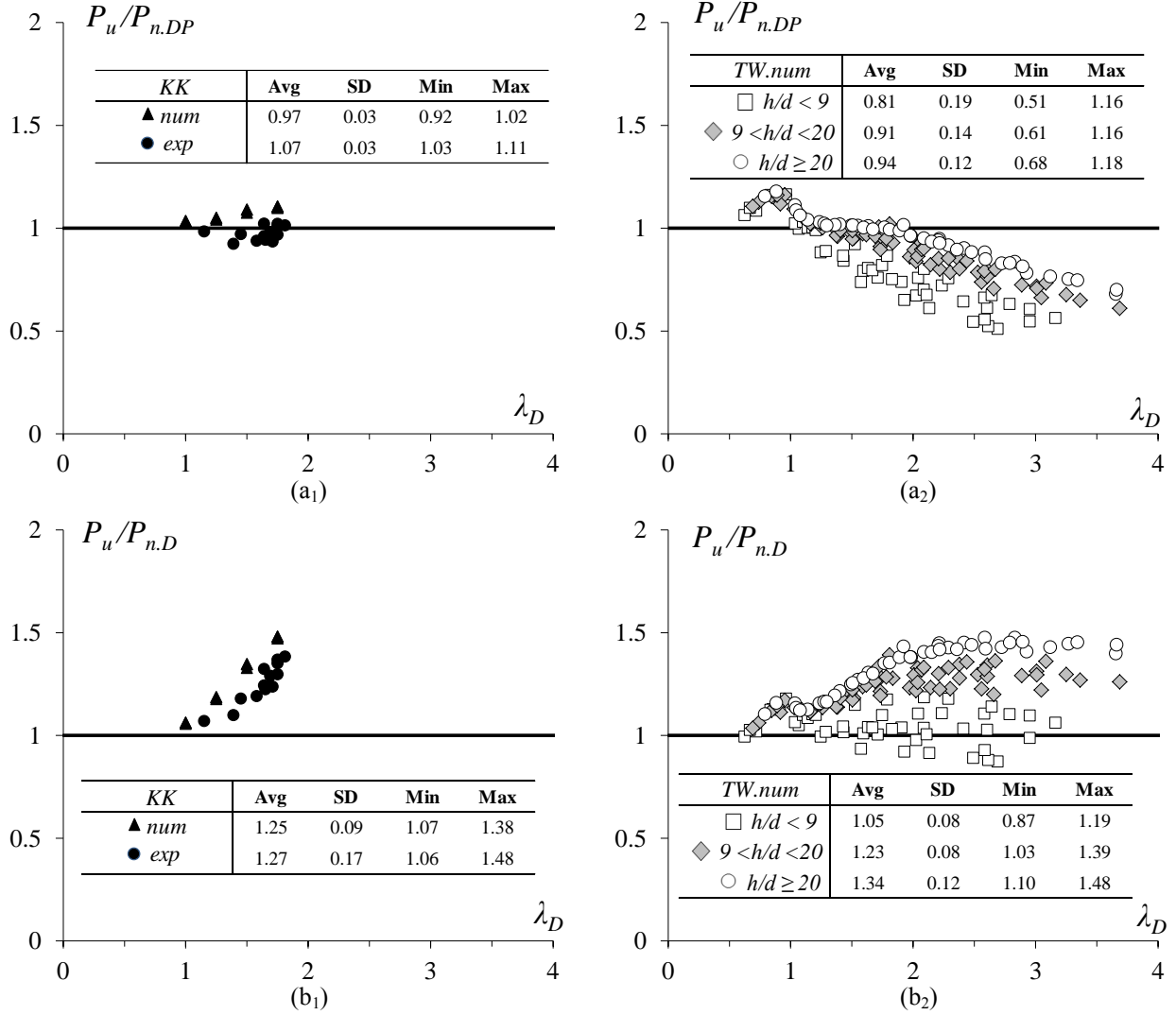


**Figure 12:** (a)  $P_u/P_{n,DP}$  and (b)  $P_u/P_{n,D}$  values and indicators concerning the SLC columns analyzed (1) by Kumar & Kalyanaraman (2014) and (2) in this work.

0.06 (standard deviation), 1.11 (maximum value) and 0.92 (minimum value). Moreover, Figs. 11(a) and 12(b<sub>1</sub>) show that the current DSM-D design curve yields extremely conservative predictions of these same failure load set, as reflected by the respective indicators: 1.26 (average), 0.13 (standard deviation), 1.48 (maximum value) and 1.06 (minimum value).

- (ii) However, the comparison between Figs. 11(a) and 11(b) provides evidence even more clear than the previous one on how premature and ill-advised was to propose such a radically new strength curve on the basis of such a small and “biased” set of failure loads. As a matter of fact, when the pool of SLC failure loads is adequately enlarged, both in column cross-section geometries and slenderness values, the inadequacy of the DSM-DP design curve becomes obvious: the indicators concerning the SLC column failure loads numerically obtained in this work<sup>10</sup> are 0.89 (average), 0.16 (standard deviation), 1.18 (maximum value) and 0.51 (minimum value), *i.e.*, clearly inadequate, particularly for columns with small  $h/d$  ratios and/or large slenderness values.

<sup>10</sup>Note that several column geometries considered by Kumar & Kalyanaraman (2014) were also dealt with in this work. But, by adopting higher yield stresses, it was possible to cover with them wider slenderness ranges.

- (iii) Nevertheless, it is fair to say that, after looking at Figs. 11(b) and 12(b<sub>1</sub>)-(b<sub>2</sub>), one also readily concludes that the DSM-D design curve underestimates (often quite considerably) the failure loads of several columns, particularly those exhibiting large  $h/d$  ratios and/or small slenderness values – Recall that all the columns analyzed by Kumar & Kalyanaraman (2014) fall into this category.
- (iv) In summary, the assessment of the DSM-D and DSM-D estimates of the failure load data dealt with in this work leads to the following conclusions:
  - (iv.1) The design curve proposed by Kumar & Kalyanaraman (2014) only provides safe and accurate failure load predictions in the low-to-moderate slenderness range ( $\lambda_D \leq 1.25$ ). For more slender SLC columns, this curve is utterly inappropriate, as it may provide quite large overestimations of several column failure loads – these overestimations grow as the web-to-lip width ratio  $h/d$  decreases and the column slenderness increases.
  - (iv.2) On the other hand, the current design curve provides safe (in many cases quite excessively) failure load predictions for the vast majority of the columns considered – the few exceptions concern a fairly slender columns with low  $h/d$  values.
  - (iv.3) The current curve (iv<sub>1</sub>) is perfectly adequate to estimate failure loads of SLC columns with low  $h/d$  values and (iv<sub>2</sub>) becomes progressively more conservative as  $h/d$  increases. Therefore, if it is deemed useful by the technical/scientific community dealing with cold-formed steel structures, it may be envisaged to develop a more refined DSM approach for the design of SLC columns against distortional failure – if this was the case, it seems that such an approach should involve  $h/d$  as a key parameter.

## 7. Concluding Remarks

This work was motivated by the experimental and numerical results recently reported by Kumar & Kalyanaraman (2014) on cold-formed steel lipped channel columns with web and flange V-shaped intermediate stiffeners, which suggest that the presence of these stiffeners may alter considerably their distortional buckling, post-buckling and collapse behaviors. In particular, a major output of their study was the development and proposal of novel DSM distortional strength curve, specifically for web-flange stiffened lipped channel columns, which lies well above the currently codified one. Since the adoption of such of curve would constitute a significant break from the existing knowledge, widely accepted by the technical/scientific community working with cold-formed steel structures, it was decided to assess the validity of the claims made by Kumar & Kalyanaraman (2014). In order to perform this task, the first step consisted of selecting several column geometries associated with “pure” distortional buckling and failure modes, which was ensured by having local and global critical buckling loads much higher than their distortional counterparts – this column set included the specimens tested by Kumar & Kalyanaraman.

After using a validated ANSYS shell finite element model to perform geometrically and materially non-linear analyses of the selected 155 stiffened lipped channel columns, the results obtained (mainly the failure load data bank gathered) made it possible to pinpoint a number of questionable assumptions and/or important limitations in the work reported by Kumar & Kalyanaraman (2014), namely:

- (i) Only 26 columns were analyzed, either experimentally or numerically, which covered a quite limited (small-to-moderate) distortional slenderness range:  $1.00-1.81$ .
- (ii) The vast majority of the above columns exhibited web-to-lip width ratio values that are either closely below or above 20.

- (iii) Without a plausible justification, the columns analyzed numerically were laterally restrained. Even if the restraints were shown not to affect much the failure loads, visible increases still occurred.

The above questionable assumptions and/or limitations provided ample evidence about the fact that the proposal of the novel DSM distortional strength curve for stiffened lipped channels was premature and ill-advised. Indeed, the failure load estimates yielded by this strength curve, for the 155 columns analyzed in this work and the 26 column analyzed by Kumar & Kalyanaraman, were shown to provide safe and accurate failure load predictions only in the low-to-moderate slenderness range ( $\lambda_D \leq 1.25$ ). For more slender SLC columns, this curve generally yields quite large failure load overestimations, which grow as the web-to-lip width ratio decreases and/or the slenderness increases. On the other hand, the analysis of the failure load predictions provided by the current DSM distortional design curve unveiled a rather different picture – in fact, it yields safe for the vast majority of the columns considered (only the failure loads of a few fairly slender columns with low  $h/d$  values were overestimated). However, these estimates were also found to become excessively safe as the column  $h/d$  value increases.

In summary, it can be concluded that the current DSM distortional design curve can continue to be used to estimate failure of web-flange stiffened cold-formed steel columns, even it provides fairly large overestimations for some column geometries – but not nearly as large as implied by the strength curve proposed by Kumar & Kalyanaraman (2014). If it is deemed useful by the technical/scientific community dealing with cold-formed steel structures to develop a more refined DSM approach for this type of columns, the results obtained in this work provided evidence that such an approach should involve the web-to-lip width ratio ( $h/d$ ) as a key parameter.

## References

- ABNT (2010). *Brazilian Standard on Design of Cold-Formed Steel Structures* (ABNT NBR 14762:2010), Brazilian Standards Association, Rio de Janeiro, RJ. (Portuguese)
- AISI (2012). *North American Specification for the Design of Cold-Formed Steel Structural Members* (NAS), American Iron and Steel Institute, Washington DC.
- AS/NZS (2005). *Cold-Formed Steel Structures*, Standards of Australia (SA) and Standards of New Zealand (SNZ), Sydney-Wellington.
- Bebiano R, Pina P, Silvestre N, Camotim D (2008a). *GBTUL 1.0 $\beta$  – Buckling and Vibration Analysis of Thin-Walled Members*, DECivil/IST, Technical University of Lisbon. (<http://www.civil.ist.utl.pt/gbt>)
- Bebiano R, Silvestre N, Camotim D (2008b). GBTUL – A code for the buckling analysis of cold-formed steel members, *Proceedings of 19<sup>th</sup> International Specialty Conference on Recent Research and Developments in Cold-Formed Steel Design and Construction* (St. Louis, 14-15/10), R LaBoube, W.-W. Yu (eds.), 61-79.
- Camotim D, Dinis PB (2013). Distortional-global interaction in lipped channel columns, *Proceedings of the Institution of Civil Engineers (ICE)-Structures and Buildings*, **166**(8), 381-391.
- Dinis PB, Camotim D (2015). Cold-formed steel columns undergoing local-distortional coupling: behaviour and direct strength prediction against interactive failure, *Computers & Structures*, **147**(January), 181-208.
- Dinis PB, Batista EM, Camotim D, Santos ES (2012). Local-distortional-global interaction in lipped channel columns: experimental results, numerical simulations and design considerations, *Thin-Walled Structures*, **61**(December), 2-13.
- Dinis PB, Young B, Camotim D (2014). L-D-G interaction in CFS lipped channel columns: experimental results, numerical simulations and design considerations, *Proceedings of Seventh European Conference on Steel and Composite Structures* (EUROSTEEL 2014 – Naples, 10-12/9), R. Landolfo, F. Mazzolani (eds.), ECCS (Brussels), 419-420. (full paper in USB Key Drive Proceedings – Paper 583)
- Garcia RAS, Landesmann A, Camotim D (2014). “Distortional buckling, post-buckling and failure of cold-formed steel stiffened lipped channel columns”, *Proceedings of the XXXVI South-American Structural Engineering Congress* (Montevideo, 19-21/11). (Portuguese)

- Hancock GJ, Kwon YB, Bernard ES (1994). Strength design curves for thin-walled sections undergoing distortional Buckling, *Journal of Constructional Steel Research*, **31**(3), 169-186.
- Kumar MV, Kalyanaraman V (2012). Design strength of locally buckling stub lipped channel columns, *Journal of Structural Engineering* (ASCE), **138**(11), 1291-1299.
- Kumar MV, Kalyanaraman V (2014). Distortional buckling of CFS stiffened lipped channel compression members, *Journal of Structural Engineering* (ASCE), **140**(12), 04014099:1-14.
- Landesmann A, Camotim D (2013). On the Direct Strength Method (DSM) design of cold-formed steel columns against distortional failure, *Thin-Walled Structures*, **67**(June), 168-187.
- Santos WS, Landesmann A, Camotim D (2014). “Application of the DSM design of pin-ended cold-formed steel columns that buckle and failure in distortional mode”, *CD-ROM Proceedings of XXXV Iberian Latin American Congress on Computational Methods in Engineering* (CILAMCE 2014 – Fortaleza, 23-26/11), paper 0573. (Portuguese).
- SAS (Swanson Analysis Systems Inc.) (2009). *ANSYS Reference Manual* (version 12.0.1).
- Schafer BW (2002). Local, distortional and Euler buckling in thin-walled columns, *Journal of Structural Engineering* (ASCE), **128**(3), 289-299.
- Schafer BW (2006). *Direct Strength Method Design Guide*, American Iron and Steel Institute (AISI) Report, Washington D.C.
- Schafer BW (2008). Review: the Direct Strength Method of cold-formed steel member design, *Journal of Constructional Steel Research*, **64**(7-8), 766-788.
- Schafer BW, Peköz T (1998). Direct strength prediction of cold-formed steel members using numerical elastic buckling solutions, *Proceedings of 14<sup>th</sup> International Specialty Conference on Cold-formed Steel Structures* (St. Louis, 15-16/10), W.-W. Yu (ed.), 69-76.
- Silvestre N, Camotim D (2006). Local-plate and distortional post-buckling behavior of cold-formed steel lipped channel columns with intermediate stiffeners, *Journal of Structural Engineering* (ASCE), **132**(4), 529-540.

## ANNEX A – DATA CONCERNING THE SLC COLUMNS ANALYZED IN THIS WORK

Tables A1 to A4 provide, for each SLC column analyzed in this work, the (i) yield stress  $f_y$ , (ii) squash load  $P_y$ , (iii) distortional slenderness  $\lambda_D$ , (iv) distortional failure load  $P_u$  and associated  $(|\delta|/t)_{lim}$  value, (v) failure load ratios  $P_u/P_{cr,D}$  and  $P_u/P_y$ , (vi) DSM distortional failure load estimates  $P_{n,D}$  and  $P_{n,DP}$ , and (vii) ratios  $P_u/P_{n,D}$  and  $P_u/P_{n,DP}$ .

**Table A1:** Numerical distortional failure loads and DSM estimates for the SLC 50-50(1)-50(2)-65-65(1) columns analyzed.

SLC	$f_y$ (MPa)	$P_y$ (kN)	$\lambda_D$	$P_u$ (kN)	$( \delta /t)_{lim}$	$\frac{P_u}{P_{cr,D}}$	$\frac{P_u}{P_y}$	$P_{n,D}$ (kN)	$P_{n,DP}$ (kN)	$\frac{P_u}{P_{n,D}}$	$\frac{P_u}{P_{n,DP}}$
50	70	6.79	0.79	6.65	0.25	0.61	0.98	6.02	5.75	1.10	1.16
	120	11.63	1.03	9.83	1.34	0.90	0.85	8.50	8.84	1.16	1.11
	250	24.23	1.49	15.83	17.11	1.45	0.65	12.68	15.62	1.25	1.01
	300	29.08	1.63	18.15	19.05	1.67	0.62	13.90	17.97	1.30	1.01
	350	33.93	1.76	20.27	20.92	1.86	0.60	14.99	20.21	1.35	1.00
	550	53.32	2.21	26.94	26.29	2.47	0.51	18.58	28.40	1.45	0.95
	750	72.70	2.58	31.61	29.68	2.90	0.43	21.41	35.81	1.47	0.88
	900	87.25	2.83	34.30	31.81	3.15	0.39	23.24	40.98	1.47	0.84
	1200	116.33	3.27	38.19	35.25	3.51	0.33	26.39	50.69	1.45	0.75
	1500	145.41	3.65	40.70	37.80	3.74	0.28	29.09	59.80	1.41	0.68
50(1)	120	11.84	0.95	10.82	0.71	0.83	0.91	9.23	9.31	1.18	1.16
	250	24.67	1.37	16.42	16.03	1.26	0.67	13.98	16.53	1.18	0.99
	400	39.47	1.74	22.72	22.34	1.74	0.58	17.73	23.64	1.28	0.96
	550	54.27	2.04	27.43	25.78	2.10	0.51	20.65	30.08	1.33	0.91
	750	74.01	2.38	32.11	29.01	2.45	0.43	23.85	37.98	1.35	0.85
	900	88.81	2.61	34.79	31.03	2.66	0.39	25.92	43.48	1.33	0.80
	1200	118.41	3.01	38.69	34.29	2.96	0.33	29.47	53.87	1.32	0.72
	1500	148.02	3.36	41.27	36.80	3.15	0.28	32.51	63.58	1.27	0.65
50(2)	120	12.06	0.84	11.61	0.49	0.67	0.96	10.33	9.97	1.12	1.16
	250	25.13	1.21	17.67	13.96	1.02	0.70	16.07	17.82	1.10	0.99
	400	40.21	1.52	23.64	21.05	1.37	0.59	20.59	25.68	1.15	0.92
	550	55.29	1.79	28.31	24.30	1.64	0.51	24.10	32.66	1.18	0.87
	750	75.40	2.09	33.13	28.36	1.92	0.44	27.95	41.29	1.19	0.80
	900	90.48	2.29	35.83	30.13	2.07	0.40	30.42	47.34	1.18	0.76
	1200	120.64	2.64	39.56	32.70	2.29	0.33	34.68	58.72	1.14	0.67
	1500	150.79	2.95	42.02	35.13	2.43	0.28	38.32	69.32	1.10	0.61
65	250	48.92	1.37	31.58	12.15	1.219	0.65	27.71	32.79	1.14	0.96
	300	58.71	1.50	35.69	13.92	1.377	0.61	30.44	37.73	1.18	0.95
	550	107.63	2.04	51.49	19.51	1.986	0.48	40.93	59.65	1.27	0.86
	750	146.76	2.38	60.49	22.31	2.334	0.41	47.28	75.30	1.28	0.80
	900	176.12	2.61	66.11	23.90	2.551	0.38	51.37	86.23	1.28	0.77
	1200	234.82	3.01	75.62	27.00	2.917	0.32	58.42	106.83	1.30	0.71
	1400	273.96	3.25	81.05	29.07	3.127	0.30	62.52	119.75	1.30	0.68
	1800	352.23	3.69	87.95	32.46	3.393	0.25	69.76	144.01	1.27	0.61
65(1)	150	30.03	0.91	27.78	0.87	0.770	0.92	24.16	24.04	1.15	1.16
	250	50.05	1.18	36.05	7.43	1.000	0.72	32.67	35.88	1.10	1.00
	550	110.10	1.75	53.98	19.69	1.497	0.49	49.14	65.76	1.10	0.82
	750	150.14	2.04	63.06	22.33	1.749	0.42	57.02	83.21	1.11	0.76
	900	180.17	2.24	68.79	24.13	1.908	0.38	62.09	95.31	1.11	0.72
	1200	240.22	2.58	78.35	27.21	2.173	0.33	70.82	118.31	1.11	0.66
	1400	280.26	2.79	83.74	29.43	2.322	0.30	75.91	132.61	1.10	0.63
	1800	360.33	3.16	90.08	32.21	2.498	0.25	84.86	159.84	1.06	0.56

**Table A2:** Numerical distortional failure loads and DSM estimates for the SLC 65(2)-65(3)-75-75(1)-80 columns analyzed.

SLC	$f_y$ (MPa)	$P_y$ (kN)	$\lambda_D$	$P_u$ (kN)	$( \delta /t)_{lim}$	$\frac{P_u}{P_{cr,D}}$	$\frac{P_u}{P_y}$	$P_{n,D}$ (kN)	$P_{n,DP}$ (kN)	$\frac{P_u}{P_{n,D}}$	$\frac{P_u}{P_{n,DP}}$
65(2)	150	30.30	0.85	28.85	0.44	0.69	0.95	25.59	24.93	1.12	1.16
	250	50.50	1.10	38.48	6.98	0.92	0.76	34.99	37.33	1.10	1.03
	550	111.09	1.63	55.31	18.31	1.33	0.50	53.15	68.65	1.04	0.81
	750	151.49	1.91	64.19	21.81	1.54	0.42	61.81	86.72	1.04	0.74
	900	181.79	2.09	69.86	23.65	1.67	0.38	67.39	99.55	1.04	0.70
	1200	242.38	2.41	79.56	26.96	1.91	0.33	76.99	123.58	1.03	0.64
	1400	282.78	2.60	84.85	29.13	2.03	0.30	82.57	138.73	1.03	0.61
	1800	363.57	2.95	91.27	32.12	2.19	0.25	92.41	167.14	0.99	0.55
65(3)	100	19.45	0.89	18.23	0.54	0.74	0.94	15.93	15.71	1.15	1.16
	150	29.17	1.09	22.92	4.82	0.93	0.79	20.37	21.65	1.12	1.06
	250	48.62	1.41	31.83	11.34	1.30	0.65	26.91	32.16	1.18	0.99
	400	77.79	1.78	43.75	14.97	1.78	0.56	34.06	46.08	1.28	0.95
	550	106.96	2.09	52.79	17.59	2.15	0.49	39.65	58.57	1.33	0.90
	750	145.86	2.44	62.16	20.01	2.53	0.43	45.76	73.91	1.35	0.84
	900	175.03	2.67	67.72	21.70	2.76	0.39	49.70	84.71	1.37	0.80
	1200	233.37	3.08	76.86	23.97	3.13	0.33	56.50	104.91	1.35	0.73
75	100	30.47	0.74	29.78	0.36	0.53	0.98	28.06	26.45	1.06	1.13
	250	76.17	1.17	56.00	6.24	1.00	0.74	50.09	54.81	1.12	1.02
	350	106.64	1.38	68.30	11.18	1.22	0.64	60.05	71.24	1.14	0.96
	550	167.58	1.73	90.09	15.64	1.61	0.54	75.43	100.65	1.19	0.90
	750	228.52	2.02	106.67	17.54	1.91	0.47	87.55	127.26	1.22	0.84
	900	274.22	2.22	116.74	19.35	2.09	0.43	95.35	145.72	1.22	0.80
	1200	365.63	2.56	133.41	21.54	2.39	0.36	108.78	180.80	1.22	0.74
	1700	517.98	3.05	155.16	25.28	2.78	0.30	127.12	234.05	1.22	0.66
75(1)	200	92.96	0.69	91.56	0.25	0.47	0.98	88.47	82.77	1.03	1.11
	300	139.44	0.85	132.84	0.34	0.68	0.95	118.41	114.74	1.12	1.16
	480	223.10	1.07	179.38	3.46	0.92	0.80	158.37	166.91	1.14	1.07
	650	302.12	1.24	216.84	5.53	1.11	0.72	187.71	211.86	1.15	1.02
	850	395.07	1.42	259.87	7.38	1.33	0.66	216.37	260.46	1.20	1.00
	950	441.55	1.50	279.98	8.08	1.43	0.63	229.08	283.77	1.22	0.99
	1200	557.75	1.69	325.40	9.42	1.67	0.58	257.46	338.76	1.27	0.96
	1800	836.63	2.07	412.50	11.73	2.11	0.49	312.84	460.32	1.32	0.90
	2200	1022.55	2.29	456.93	12.89	2.34	0.45	343.47	534.97	1.33	0.85
	2800	1301.42	2.58	506.99	14.19	2.60	0.39	383.44	640.98	1.32	0.79
	3500	1626.78	2.89	547.43	15.64	2.81	0.34	423.82	755.87	1.30	0.72
80	250	138.21	0.72	131.53	0.49	0.49	0.95	129.08	121.17	1.02	1.09
	550	304.07	1.07	227.23	4.03	0.85	0.75	216.36	227.49	1.05	1.00
	750	414.64	1.25	256.06	5.45	0.96	0.62	257.47	289.72	0.99	0.88
	1200	663.42	1.58	307.42	9.79	1.15	0.46	328.89	416.06	0.93	0.74
	1800	995.14	1.93	369.20	12.47	1.38	0.37	400.96	566.75	0.92	0.65
	2200	1216.28	2.13	403.13	13.95	1.51	0.33	440.79	659.79	0.92	0.61
	3000	1658.56	2.49	452.92	16.29	1.69	0.27	508.50	831.78	0.89	0.54
	3500	1934.98	2.69	475.86	17.57	1.78	0.25	545.20	932.89	0.87	0.51

**Table A3:** Numerical distortional failure loads and DSM estimates for the SLC 90-90(1)-90(2)-90(3)-100 columns analyzed.

SLC	$f_y$ (MPa)	$P_y$ (kN)	$\lambda_D$	$P_u$ (kN)	$( \delta /t)_{lim}$	$\frac{P_u}{P_{cr,D}}$	$\frac{P_u}{P_y}$	$P_{n,D}$ (kN)	$P_{n,DP}$ (kN)	$\frac{P_u}{P_{n,D}}$	$\frac{P_u}{P_{n,DP}}$
90	200	113.89	0.62	111.60	0.22	0.382	0.98	112.23	105.23	0.99	1.06
	550	313.20	1.04	243.03	0.50	0.833	0.78	228.25	237.19	1.06	1.02
	850	484.04	1.29	296.51	1.71	1.016	0.61	291.34	333.44	1.02	0.89
	1050	597.93	1.43	330.71	11.17	1.133	0.55	325.58	392.91	1.02	0.84
	1300	740.30	1.59	366.41	12.53	1.256	0.49	362.89	462.89	1.01	0.79
	1500	854.19	1.71	391.44	13.17	1.342	0.46	389.55	515.89	1.00	0.76
	2100	1195.87	2.02	447.57	15.04	1.534	0.37	457.98	665.98	0.98	0.67
	3500	1993.12	2.61	510.61	18.73	1.750	0.26	579.62	975.88	0.88	0.52
90(1)	250	137.87	0.92	123.02	0.53	0.75	0.89	110.56	109.90	1.11	1.12
	400	220.58	1.16	162.82	5.996	0.99	0.74	146.01	159.33	1.11	1.02
	550	303.30	1.36	203.81	8.399	1.24	0.67	173.48	203.97	1.18	1.00
	750	413.60	1.59	251.76	10.632	1.53	0.61	203.37	258.61	1.23	0.97
	1000	551.46	1.83	299.44	12.335	1.83	0.54	234.23	322.33	1.28	0.93
	1200	661.75	2.01	330.64	13.293	2.02	0.50	255.54	369.43	1.30	0.89
	1450	799.62	2.21	363.11	14.523	2.21	0.45	279.23	425.86	1.30	0.85
	1900	1047.78	2.53	409.57	16.023	2.50	0.39	316.09	521.23	1.30	0.79
90(2)	250	135.62	1.08	107.55	2.15	0.92	0.79	95.79	101.06	1.12	1.06
	400	216.98	1.36	148.23	8.937	1.26	0.68	124.04	145.92	1.19	1.02
	550	298.35	1.60	186.82	12.079	1.59	0.63	146.01	186.00	1.28	1.00
	850	461.09	1.98	249.19	15.526	2.13	0.54	180.43	259.32	1.39	0.96
	1000	542.46	2.15	273.75	16.596	2.34	0.50	194.76	292.90	1.41	0.93
	1200	650.95	2.36	300.93	18.120	2.57	0.46	211.90	335.44	1.43	0.90
	1450	786.57	2.59	328.57	19.579	2.80	0.42	230.97	386.64	1.43	0.85
	1850	1003.55	2.93	362.81	21.429	3.10	0.36	257.61	462.99	1.41	0.78
90(3)	300	168.14	1.03	139.85	1.19	0.88	0.83	123.15	127.86	1.14	1.09
	450	252.21	1.26	175.86	9.095	1.11	0.70	154.79	175.59	1.14	1.00
	650	364.30	1.52	221.78	12.746	1.40	0.61	187.61	232.67	1.18	0.95
	850	476.39	1.73	260.43	14.891	1.64	0.55	214.41	286.12	1.22	0.91
	1100	616.51	1.97	299.07	16.854	1.89	0.49	242.76	347.60	1.23	0.86
	1300	728.60	2.14	323.80	18.203	2.04	0.44	262.62	394.32	1.23	0.82
	1500	840.69	2.30	344.36	19.012	2.17	0.41	280.64	438.87	1.23	0.78
	2000	1120.92	2.66	383.89	21.461	2.42	0.34	319.91	543.53	1.20	0.71
100	150	59.16	1.29	41.27	9.64	1.17	0.70	35.45	40.75	1.16	1.01
	250	98.59	1.67	59.94	14.672	1.70	0.61	46.07	60.22	1.30	1.00
	350	138.03	1.98	74.93	18.035	2.12	0.54	54.21	77.63	1.39	0.97
	440	173.52	2.22	85.62	19.674	2.42	0.49	60.35	92.21	1.43	0.93
	550	216.90	2.48	96.39	21.486	2.73	0.44	66.87	109.00	1.45	0.88
	750	295.78	2.89	111.94	24.132	3.17	0.38	76.88	137.43	1.45	0.81
	1000	394.37	3.34	126.90	26.771	3.59	0.32	87.29	169.94	1.45	0.75
	1200	473.24	3.66	136.28	28.843	3.86	0.29	94.50	194.32	1.45	0.70

**Table A4:** Numerical distortional failure loads and DSM estimates for the SLC 100(1)-120-120(1)-120(2)-120(3)-140-140(1)-150 columns analyzed.

SLC	$f_y$ (MPa)	$P_y$ (kN)	$\lambda_D$	$P_u$ (kN)	$( \delta /t)_{lim}$	$\frac{P_u}{P_{cr,D}}$	$\frac{P_u}{P_y}$	$P_{n,D}$ (kN)	$P_{n,DP}$ (kN)	$\frac{P_u}{P_{n,D}}$	$\frac{P_u}{P_{n,DP}}$
100(1)	250	179.56	1.04	147.65	1.39	0.90	0.82	130.05	135.98	1.14	1.09
	350	251.39	1.24	181.95	6.32	1.10	0.72	157.25	176.29	1.16	1.03
	450	323.22	1.40	218.56	8.52	1.33	0.68	179.74	214.49	1.22	1.02
	550	395.04	1.55	253.28	10.19	1.54	0.64	199.19	250.00	1.27	1.01
	750	538.69	1.81	314.48	12.54	1.91	0.58	232.15	316.55	1.35	0.99
	1000	718.26	2.09	374.67	14.74	2.27	0.52	266.24	393.32	1.41	0.95
	1200	861.91	2.29	413.89	15.79	2.51	0.48	289.81	450.93	1.43	0.92
	1700	1221.04	2.72	485.53	18.37	2.95	0.40	339.55	585.34	1.43	0.83
120	120	63.87	0.67	63.25	0.32	0.44	0.99	61.62	57.46	1.03	1.10
	250	133.07	0.96	121.20	0.59	0.85	0.91	102.79	104.23	1.18	1.16
	350	186.30	1.14	135.82	2.18	0.95	0.73	125.21	135.60	1.09	1.00
	550	292.75	1.43	166.57	17.41	1.16	0.57	159.71	192.37	1.04	0.87
	750	399.21	1.67	194.07	22.08	1.35	0.49	186.78	243.85	1.04	0.80
	900	479.05	1.83	210.64	24.54	1.47	0.44	204.17	280.00	1.03	0.75
	1200	638.74	2.11	235.25	28.55	1.64	0.37	234.08	348.12	1.00	0.68
	1800	958.10	2.58	261.97	33.82	1.83	0.27	282.05	471.89	0.93	0.56
120(1)	285	160.96	1.48	101.91	17.79	1.39	0.63	84.61	104.09	1.20	0.98
120(2)	284	166.03	1.72	100.60	18.71	1.79	0.61	75.30	99.99	1.33	1.01
120(3)	283	174.01	1.81	104.37	20.00	1.96	0.60	74.99	102.25	1.39	1.02
140	285	176.72	1.62	106.13	18.38	1.57	0.60	85.25	109.52	1.25	0.97
140(1)	285	181.69	1.92	105.45	19.65	2.14	0.58	73.54	103.74	1.43	1.02
150	120	138.63	0.88	132.53	0.38	0.74	0.96	114.33	112.51	1.16	1.18
	200	231.05	1.14	175.17	6.63	0.98	0.76	155.43	168.17	1.13	1.04
	250	288.81	1.27	204.78	9.32	1.15	0.71	175.73	200.36	1.17	1.02
	350	404.33	1.51	263.22	13.16	1.48	0.65	209.51	259.04	1.26	1.02
	550	635.38	1.89	361.61	17.61	2.03	0.57	261.80	365.59	1.38	0.99
	750	866.43	2.2	435.17	20.33	2.44	0.50	303.02	462.49	1.44	0.94
	900	1039.72	2.42	478.64	21.93	2.69	0.46	329.57	529.02	1.45	0.90
	1200	1386.29	2.79	545.12	24.54	3.06	0.39	375.33	655.94	1.45	0.83